

Logarithmic profiles of velocity in stably stratified atmospheric boundary layers

Yu Cheng*

*Department of Earth and Planetary Sciences,
Harvard University, Cambridge,
Massachusetts, USA*

Andrey Grachev

*Boundary Layer Research Team/Atmospheric Dynamics & Analytics Branch,
DEVCOM Army Research Laboratory, WSMR, NM, USA*

Chiel van Heerwaarden

*Meteorology and Air Quality Group,
Wageningen University,
Wageningen, the Netherlands*

(Dated: September 16, 2022)

Abstract

The universal velocity log law first proposed by von Kármán in the near-wall region of turbulent shear flows is one of the cornerstones of turbulence theory. When buoyancy effects are important, the universal velocity log law is typically believed to break down according to Monin-Obukhov similarity theory (MOST), which has been used in almost all global weather and climate models to describe the dependence of the mean velocity profiles on buoyancy in the atmospheric boundary layer. In contrast to MOST, we propose new logarithmic profiles of near-wall mean velocity in the stably stratified atmospheric boundary layers based on direct numerical simulations and field observations across a wide range of buoyancy effects. We find that buoyancy does not change the logarithmic nature of velocity profiles but instead modifies the slope of the log law in stably stratified conditions.

I. INTRODUCTION

In the near-wall region of turbulent shear flows, there exists a universal logarithmic velocity profile [1, 2], characterized by a constant slope between mean velocity and the logarithm of the distance to the wall. The universal velocity log law has been supported by laboratory measurements of pipe flow [3] and boundary layer [4], atmospheric observations [5], and direct numerical simulations (DNS) [6, 7] of turbulent shear flows. When turbulent flow is influenced by buoyancy, the mean velocity may not be adequately described by the universal log law. To address the buoyancy effects, Monin-Obukhov similarity theory (MOST) was proposed to revise the universal velocity log law using stability correction functions of the distance to the wall z and the Obukhov length L [8] based on dimensional analysis [9]. MOST has been used to describe buoyancy corrections of the mean velocity profile and to provide velocity and momentum flux in the atmospheric surface layer, roughly the lowest 10% of the atmospheric boundary layer (ABL) [10], in almost all numerical weather prediction and climate models [11–14]. According to MOST, the mean velocity profile is not logarithmic in stably stratified conditions as compared to von Kármán’s universal log law due to buoyancy corrections.

The stably stratified conditions are frequently observed over land at night [15] and in

* yc2965@columbia.edu

polar regions of the Earth [16] when the air is cooled by the land surface. Stably stratified turbulence in the ABL is very difficult to be represented [17–19] in numerical weather prediction (NWP) and climate models [20–22]. The turbulence representation in the ABL is especially important for the Arctic as climate change is amplified there [23]. The difficulty of representing stably stratified turbulence is partly due to the widely known failure of MOST in the atmospheric surface layer in very stable conditions [15, 24]. In particular, MOST does not capture the mean velocity profile when buoyancy-driven stratification is significant as was shown in field observations of the very stable ABL [25–30].

Based on a reformulation of MOST, Grachev et al. [16] proposed a similarity theory using the Dougherty-Ozmidov length scale L_O [31, 32], which is typically regarded as the outer scale of isotropic turbulence in stably stratified conditions [33–36]. It is thus possible that some important length scales might be missing in the dimensional analysis of MOST when stably stratified turbulence is considered, as was shown in convective conditions [37, 38]. The strength of stratification is typically described by the stability parameter z/L according to MOST, where $L = \frac{u_\tau^3}{\frac{\kappa g}{\Theta_r} u_\tau \theta_*}$, u_τ is the friction velocity, κ is the von Kármán constant, g is the gravitational acceleration, Θ_r is a reference potential temperature, $\theta_* \equiv \frac{\nu_\theta}{u_\tau} \frac{\partial \Theta}{\partial z} \Big|_{z=0}$ is a scaling temperature, and ν_θ is the thermal diffusivity. When buoyant stratification increases, z/L increases. In addition, Grachev et al. [16] showed that z/L_O may also characterize buoyancy effects, where L_O is the Dougherty-Ozmidov length scale [31, 32].

It is worth noting that the collapse of turbulence in stably stratified conditions can be indicated by the parameter $\frac{L}{\delta_v} = \frac{L u_\tau}{\nu}$ [39], where δ_v is the viscous length scale, and ν is the kinematic viscosity. L/δ_v can characterize both buoyancy effects (i.e., the inverse of gradient Richardson number) [40] and Reynolds number effects (i.e., the scale separation between L and δ_v) [39]. We can write $\frac{L}{\delta_v} = \frac{z_i/\delta_v}{z_i/L}$, where z_i is the boundary layer height. $\frac{z_i}{\delta_v} = \frac{u_\tau z_i}{\nu}$ can represent Reynolds number effects, and $\frac{z_i}{L}$ can represent buoyancy effects (e.g., in the convective boundary layer [38]). We will show that $\frac{z_i}{\delta_v}$ and $\frac{z_i}{L}$ can be used to constrain the slope of our proposed velocity log law.

Recently, the logarithmic temperature profiles have been reported in the near-wall regions of turbulent Rayleigh-Bénard convection [41–43], vertical natural convection [44], and convective ABL [38], which is in contrast with the breakdown of a log law according to MOST. Thus, the logarithmic nature does not necessarily break down under the influence of buoyancy. In this study, we aim to investigate the existence of logarithmic velocity profiles in

the stably stratified ABL and the possible dependence of velocity profiles on other stability parameters (or length scales) using high-resolution DNS experiments and field observations.

II. METHODS

A. Direct numerical simulations

Large eddy simulations (LESs) [45–47] have been widely used to study the ABL. However, subgrid-scale turbulence models [48, 49] may lead to uncertainties near the wall and LESs might have difficulties in simulating strongly stratified turbulence [39, 50]. In addition, wall-modeled LES for the ABL usually invokes MOST [45, 51–54]. Moreover, turbulence spectra are often not well resolved [36] since the Dougherty-Ozmidov scale is typically not resolved in LESs [34, 55, 56] except possibly in a few studies [57]. Recently, DNS has been used to study the stably stratified ABL [36, 39, 40, 58, 59], although the Reynolds number is not as high as that in the real ABL. To obtain high-resolution velocity profiles in the near-wall region, DNSs of the stably stratified Ekman layers are conducted in this study.

The incompressible Navier-Stokes equations with Boussinesq approximation are solved [60]. Periodic boundary conditions are employed in the horizontal (x and y) directions. Firstly, we simulate a turbulent Ekman layer flow [61] over a smooth surface in the absence of buoyancy as in previous studies [58, 59]. The three simulations of neutral Ekman layer flow named ReD900, ReD1800 and ReD2700 are forced with varying mean geostrophic wind. The grid points are $320 \times 320 \times 1664$ for the dataset ReD900, $640 \times 640 \times 3328$ for the dataset ReD1800, $960 \times 960 \times 4992$ for the dataset ReD2700 in streamwise (x), spanwise (y), and vertical directions (z), respectively. The Reynolds number is $Re_D = \frac{U_g D}{\nu}$, where U_g is the geostrophic wind speed, $D = (2\nu/f)^{1/2}$ is the laminar Ekman layer depth, ν is the kinematic viscosity, and f is the Coriolis parameter. Similarly to previous experiments [58, 59], a neutral velocity log law of the Ekman layer is obtained after $ft = 5.9, 6.0$ and 13.6 for ReD900, ReD1800 and ReD2700, respectively. Then we add a cooling surface buoyancy flux B_0 to generate various stably stratified conditions. The boundary conditions for the temperature field are zero heat flux at the top of the computational domain. At the top 25% of the computation domain, a sponge layer is added to prevent reflection of gravity waves [47]. The near-surface stability is measured by normalized Obukhov length $L^+ = \frac{L}{\delta_v} = \frac{u_\tau^3}{\frac{\kappa g}{\Theta_\tau} u_\tau \theta_*} \frac{u_\tau}{\nu}$.

The initial $L^+(t = 0)$ is used to measure the strength of imposed stratification, which is computed from u_τ in the neutral Ekman layer before the cooling surface buoyancy flux B_0 is applied. Details of the DNS setup can be found in Cheng et al. [36] and the code is described in Heerwaarden et al. [60].

We note that turbulence decays fast in the stably stratified Ekman layer [59], thus we only analyze the periods when $\frac{L_0}{\eta} > 1$ for the possible existence of Kolmogorov’s energy cascade [36], where $\eta = (\nu^3/\epsilon)^{1/4}$ is the Kolmogorov scale [62] and ϵ is the turbulent kinetic energy (TKE) dissipation rate. The friction Reynolds number $Re_\tau = u_\tau \delta_t / \nu$ at the selected time step of the DNS experiments ReD900 ($L^+ = 160$), ReD1800 ($L^+ = 800$), ReD1800 ($L^+ = 3200$), and ReD2700 ($L^+ = 160$) are 861, 1208, 1026 and 3122, respectively, where $\delta_t = u_\tau / f$ is the turbulent Ekman layer length scale. Following the suggestion of Shah and Bou-Zeid [58], we compute the boundary layer height z_i in DNS experiments as the height where maximum of velocity occurs. The eight stably stratified DNS experiments are described in Table I.

B. Field observations

A tower of 213 m has been installed in the Cabauw Experimental Site for Atmospheric Research (CESAR) [63, 64] (4.926° E, 51.97° N) in the Netherlands, where multi-level turbulence observations at 10 m, 20 m, 40 m, 80 m, 140 m and 200 m above a grass field are available in the ABL. We download a number of 30-minute data segments between 1:00 and 5:00 UTC in July 2019 from the CESAR data archive as the raw data, which has been quality controlled [64]. These include velocity measurements from cup-anemometers at multiple levels and surface flux measurements from sonic anemometers at 3 m. Through detecting the top of an elevated aerosol layer, the boundary layer height z_i is measured by the Lufft CHM 15k ceilometer [65]. We calculate the average of ABL height over each 30-minute segment as the raw data.

The raw data satisfying the following two conditions are further used to characterize the velocity profile: (1) the mean surface heat flux in the 30-minute sampling period has to be negative (i.e., heat transferred from air to ground); and (2) the boundary layer height z_i is larger than 800 m. The first condition is used to select stably stratified ABL. The second condition is used to ensure that we include as many measurements as possible (especially

TABLE I. Key parameters of the simulated stably stratified ABLs. $Re_\tau = \frac{u_\tau \delta_t}{\nu}$ is the friction Reynolds number, u_τ is the friction velocity, δ_t is the turbulent Ekman layer length scale, ν is the kinematic viscosity, z_i is the boundary layer height determined from the height where maximum of velocity occurs, L is the Obukhov length, L_x , L_y and L_z are the domain sizes in the x , y and z directions, respectively. $\Delta_x^+ = (\Delta_x u_*)/\nu$, Δ_y^+ and Δ_z^+ are the spatial grid resolutions denoted by inner units in the x , y and z directions, respectively. κ_u is the inverse of the velocity log law slope. The range of velocity log law is also indicated using z^+ and $\frac{z}{L}$.

DNS data	Re_D	$Re_\tau = \frac{u_\tau \delta_t}{\nu}$	$\frac{z_i}{L}$	Δ_x^+ (Δ_y^+)	Δ_z^+	L^+	κ_u	Log-law range in z^+	Log-law range in $\frac{z}{L}$
ReD900	900	861	5.4	6.5	0.82	160	0.33	81 ~ 100	1.01 ~ 1.25
ReD900	900	806	2.2	6.3	0.80	480	0.28	59 ~ 70	0.30 ~ 0.35
ReD900	900	548	0.9	5.2	0.66	1600	0.28	83 ~ 94	0.26 ~ 0.30
ReD1800	1800	1208	6.6	3.8	0.49	800	0.20	81 ~ 97	0.84 ~ 1.01
ReD1800	1800	1088	2.0	3.6	0.46	1600	0.17	86 ~ 103	0.55 ~ 0.66
ReD1800	1800	1026	3.7	3.5	0.45	3200	0.16	112 ~ 131	0.40 ~ 0.47
ReD2700	2700	3122	42.0	4.1	0.52	160	0.24	100 ~ 121	3.04 ~ 3.67
ReD2700	2700	1624	11.2	3.0	0.38	1600	0.15	102 ~ 122	1.16 ~ 1.38

those at 200 m) within the atmospheric surface layer through prescribing large boundary layer height z_i . These two conditions lead to 40 different stably stratified 30-minute periods.

III. RESULTS

A. Existence of a velocity log law

The normalized mean velocity $\frac{U}{u_\tau}$ fits a log law with $z^+ \equiv \frac{z}{\delta_v}$ in the DNS datasets (Fig. 1). The coefficient of determination R^2 for $\frac{U}{u_\tau}$ and $\log(z^+)$ is 1.00 for the selected vertical layer (according to Fig. 2) near the wall across the DNS datasets. Following Lee and Moser (2015) [6], we use a plateau of $\frac{z}{u_\tau} \frac{\partial U}{\partial z}$ to more clearly indicate the existence of a velocity log law (Fig. 2). The black dashed line (plateau) in Fig. 2 is used to characterize the vertical layer where the velocity log law is identified (as detailed in Table 1).

In the identified log law layer, the variations of turbulent momentum flux $\overline{w'u'}$ defined as $\frac{\max(\overline{w'u'}) - \min(\overline{w'u'})}{\max(\overline{w'u'})}$ are 4.7% (ReD900, $L^+=160$), 10.6% (ReD1800, $L^+=800$), 5.3% (ReD1800, $L^+=3200$), and 4.3% (ReD2700, $L^+=160$), respectively. This is consistent with the definition of constant-flux layer [10], where flux variations are on the order of 10%. This constant momentum flux zone is similar to the atmospheric surface layer, where the variation of turbulent fluxes should scale with the ratio of the atmospheric surface layer height to the ABL height [66], roughly 10%. The coexistence of a velocity log law and constant momentum flux in the DNS datasets (Fig. 1) resembles that in turbulent shear flows [67].

As shown in Table 1, the range of Reynolds number of the DNS experiments is $548 \leq Re_\tau \leq 3122$, or equivalently $276 \leq z_i/\delta_v \leq 1345$. The vertical layers of velocity log law vary in different DNS experiments but all fall in the range $59 \leq z^+ \leq 122$. According to Marusic et al. [68], the universal velocity log law of turbulent shear flows in the absence of buoyancy effects is found in the range $3(z_i/\delta_v)^{1/2} < z^+ < 0.15z_i/\delta_v$, which corresponds to $50 \leq z^+ \leq 202$ in our DNS experiments. Thus the range of the stably stratified velocity log law roughly falls within that of neutral velocity log law, although the influence of buoyancy effects cannot be neglected in our DNS experiments. In addition, the stably stratified velocity log law is found when $\frac{z}{L} > 3$ (in ReD2700, $L^+=160$) using the MOST stability parameter. However, MOST suggests that velocity profiles will significantly deviate from a log law in such stably stratified conditions (Fig. 2d). In fact, the stability correction functions of MOST are only defined in the range $0 < \frac{z}{L} < 1$ in stably stratified conditions due to its poor behaviour in more stratified conditions [69]. Therefore, the proposed velocity log law is fundamentally different from MOST and can be applied to a wider range of buoyant

conditions.

The slopes of the proposed velocity log law are $\frac{1}{0.82\kappa}$ (ReD900, $L^+=160$), $\frac{1}{0.50\kappa}$ (ReD1800, $L^+=800$), $\frac{1}{0.41\kappa}$ (ReD1800, $L^+=3200$), and $\frac{1}{0.61\kappa}$ (ReD2700, $L^+=160$), respectively (Fig. 1). In comparison, the slope of the universal log law for mean velocity in turbulent shear flows is constant, i.e., $\frac{1}{\kappa}$ [68]. The variations of the slope of proposed velocity log law is due to buoyancy effects as well as Reynolds number effects. Similar dependence of the slope on buoyancy has been found in temperature log laws in the convective boundary layers [38] and Rayleigh-Bénard convection [41]. The slope of the proposed velocity log law will be revisited later.

In addition to the DNS experiments, we analyze field observations of the stably stratified ABL in the Cabauw experiment, which are at higher Reynold number ($1.4 \times 10^6 \leq \frac{z_i}{\delta_v} \leq 2.1 \times 10^7$). A linear relation is fitted between the normalized velocity $\frac{U-U_{h1}}{u_\tau}$ and $\log(z^+)$ in the 4 sampled periods (Fig. 3), where U is the temporally averaged wind speed at heights of 20 m, 40 m, 80 m, 140 m, and 200 m in a 30-minute period, and U_{h1} is the averaged wind speed at 10 m. The coefficient of determination for $\frac{U-U_{h1}}{u_\tau}$ and $\log(z^+)$ satisfies the condition that $R^2 > 0.88$ in all the selected 40 periods, indicating the linear relation between $\frac{U-U_{h1}}{u_\tau}$ and $\log(z^+)$ and thus the presence of a velocity log law. We also compare the velocity profile based on MOST [70, 71] with field observations and find substantial deviations across stably stratified conditions in the range $0.22 \leq z/L \leq 15.68$ (Fig. 3), where $z = 10$ m (at one level of tower observations). The field observations in the real ABL confirm the existence of the velocity log law observed in our DNS experiments.

It is worth noting that few studies have investigated the logarithmic nature of the mean velocity profile in the stably stratified ABL. This is partly due to the sparse measurements in the vertical direction. In addition, large uncertainties remain in the observations of the stable ABL since instruments often operate near their threshold levels due to small turbulence intensities [72–75]. Unlike DNS experiments, a plateau of $\frac{z}{u_\tau} \frac{\partial U}{\partial z}$ can hardly be identified in field observations to support a velocity log law. Moreover, field observations are often analyzed within the framework of MOST since MOST is still regarded as the foundation of ABL turbulence theory [69].

B. Slope of the velocity log law

1. Dimensional analysis

Fully developed stably stratified boundary layer flow can be described by ν , u_τ , z , θ_* and the boundary layer height z_i . These variables can form 3 non-dimensional groups:

$$\frac{z}{L} = \frac{\kappa g \theta_*}{\Theta_r} \frac{z}{u_\tau^2}, \quad (1)$$

$$\frac{z_i}{L} = \frac{\kappa g \theta_*}{\Theta_r} \frac{z_i}{u_\tau^2}, \quad (2)$$

and

$$\frac{z_i}{\delta_v} = \frac{u_\tau z_i}{\nu}. \quad (3)$$

The mean velocity profile can be written as

$$U = u_\tau F_0 \left(\frac{z}{L}, \frac{z_i}{L}, \frac{z_i}{\delta_v} \right), \quad (4)$$

where F_0 is a function of $\frac{z}{L}$, $\frac{z_i}{L}$, and $\frac{z_i}{\delta_v}$. Following the argument for velocity gradient in Pope (2000) [76], $\frac{\partial U}{\partial z}$ can be written as

$$\frac{\partial U}{\partial z} = \frac{u_\tau}{z} \Phi \left(\frac{z}{L}, \frac{z_i}{L}, \frac{z_i}{\delta_v} \right). \quad (5)$$

According to the DNS datasets, $\frac{z}{u_\tau} \frac{\partial U}{\partial z}$ is independent of z in the log law region. For the existence of a velocity log law, Φ has to be independent of $\frac{z}{L}$, leading to

$$\frac{\partial U}{\partial z} = \frac{u_\tau}{z} \Phi \left(\frac{z_i}{L}, \frac{z_i}{\delta_v} \right). \quad (6)$$

We denote $\frac{1}{\kappa_u} \equiv \Phi \left(\frac{z_i}{L}, \frac{z_i}{\delta_v} \right)$ and obtain

$$\frac{\partial U}{\partial z} = \frac{u_\tau}{z} \frac{1}{\kappa_u}. \quad (7)$$

After integration from a reference height z_r to z , we have

$$\frac{U - U_{z_r}}{u_\tau} = \frac{1}{\kappa_u} \log \left(\frac{z}{z_r} \right). \quad (8)$$

Equation (8) is just the velocity log law since κ_u is independent of z and is a function of $\frac{z_i}{L}$ and $\frac{z_i}{\delta_v}$. This dimensional analysis points out the relevant parameters that determine the slope of the proposed velocity log law, which should be calibrated from numerical experiments or field observations.

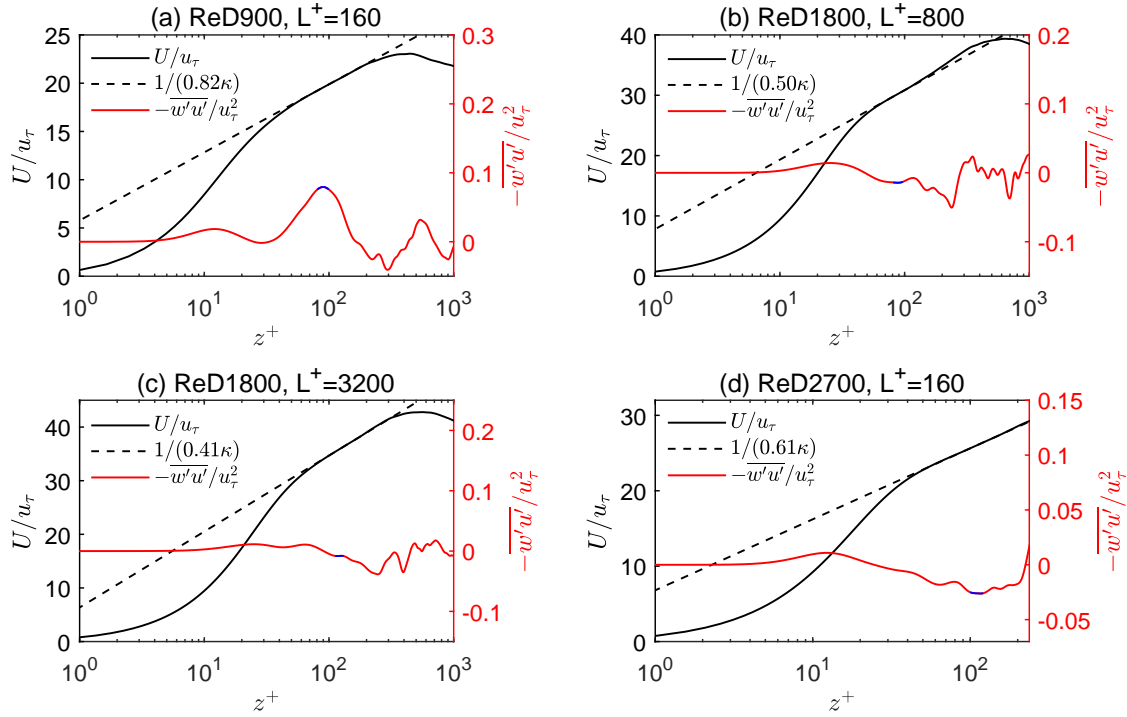


FIG. 1. Normalized velocity U/u_τ and momentum flux $-\overline{w'u'}/u_\tau^2$ in the vertical direction of the DNS experiments. The blue line denotes the normalized momentum flux $-\overline{w'u'}/u_\tau^2$ in the velocity log law region.

2. DNS and field observations

The DNS and Cabauw datasets suggest that κ_u/κ decreases nonlinearly with increasing z_i/L (Fig. 4a). That is to say, as buoyancy effects increase (i.e., z_i/L increases), the slope of the stably stratified velocity log law deviates more from that of the neutral channel flow.

When z_i/δ_v increases from $\sim 10^3$ (DNS datasets) to $\sim 10^7$ (field observations), κ_u/κ does not seem to show a monotonic trend (Fig. 4b). At high Reynolds number ($1.4 \times 10^6 \leq z_i/\delta_v \leq 2.1 \times 10^7$), κ_u/κ in Cabauw observations can be assumed to be independent of Reynolds number thus buoyancy effects dominates. In comparison, the Reynolds number is $276 \leq z_i/\delta_v \leq 1345$ for the DNS datasets, thus there is a wide separation of Reynolds number between field observations and DNS experiments. The range of MOST stability parameter in the identified log law range are $0.22 < z/L < 313.70$ and $0.26 < z/L < 3.67$ for the Cabauw and DNS datasets, respectively. Therefore, both larger Reynolds number and stronger buoyancy effects can be found in Cabauw observations. More accurate measurements of turbulent

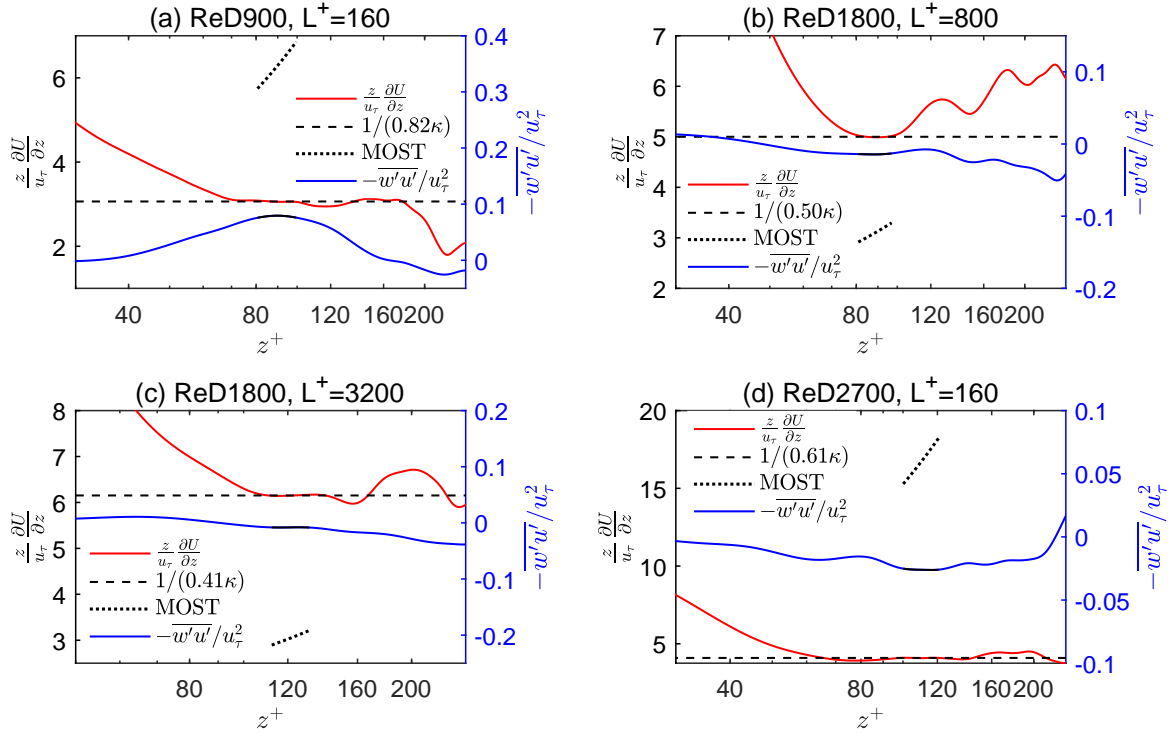


FIG. 2. Vertical profiles of normalized velocity gradient ($z/u_\tau \partial u / \partial z$) (equal to $1/\kappa_u$) in DNS datasets. The widely used Monin-Obukhov similarity function of Businger et al. [77] denoted by “MOST” is also shown.

fluxes and denser measurements of velocity in the vertical direction over a wider range of Reynolds numbers and stably stratified conditions as well as laboratory experiments (e.g., Williams et al. [78]) will better constrain κ_u in the ABL.

3. Asymptotic analysis

At sufficiently high Reynolds numbers like the field observations, we conduct asymptotic analysis for the slope κ_u in the “neutral limit” and “strongly stratified limit” by neglecting the Reynolds number effects.

In the neutral limit (where there is no buoyancy) at sufficiently high Reynolds numbers, $z_i/L \rightarrow 0$, we expect that $\kappa_u/\kappa \rightarrow 1$ since von Kármán’s universal log law is recovered.

In the strongly stratified limit at sufficiently high Reynolds numbers, $z_i/L \rightarrow \infty$ and

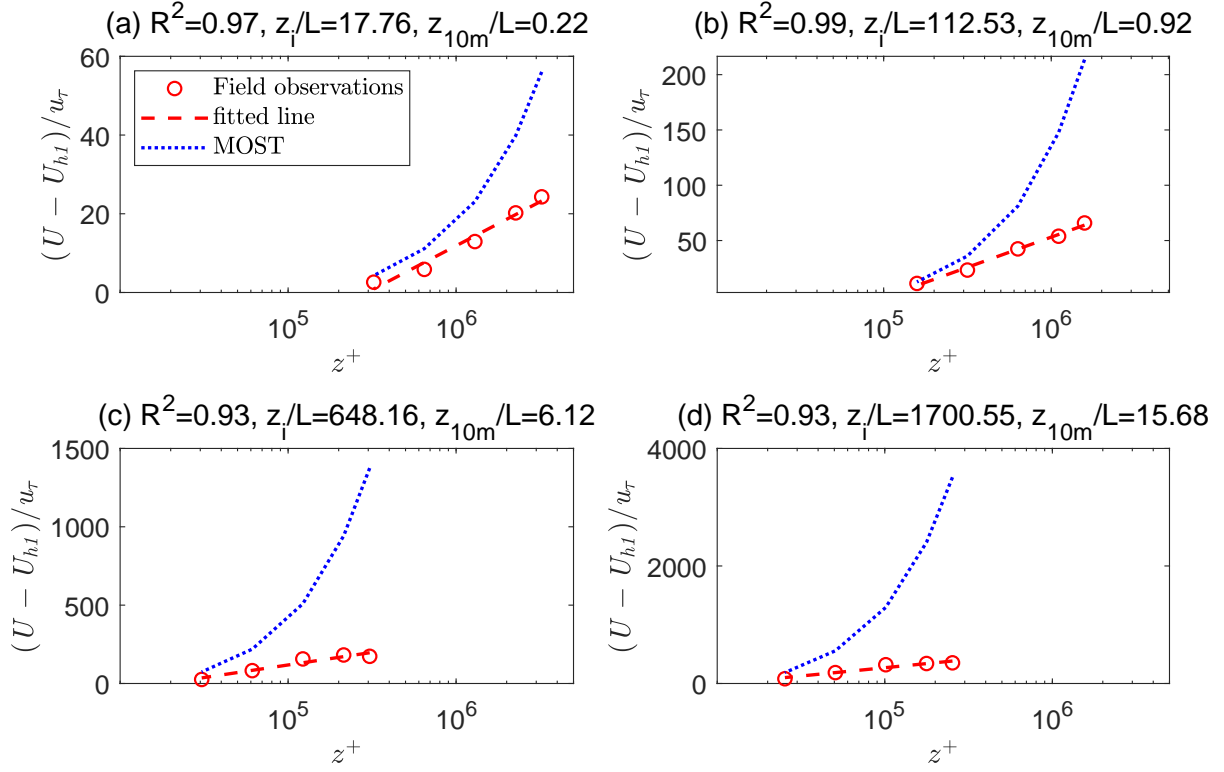


FIG. 3. Normalized velocity $\frac{U-U_{h1}}{u_{\tau}}$ in the vertical direction of Cabauw observations. R^2 denotes the coefficient of determination for $\frac{U-U_{h1}}{u_{\tau}}$ and $\log(z^+)$, and z_{10m}/L denotes the stability parameter z/L at the height 10 m. “MOST” denotes the computed velocity profiles based on Monin-Obukhov similarity theory.

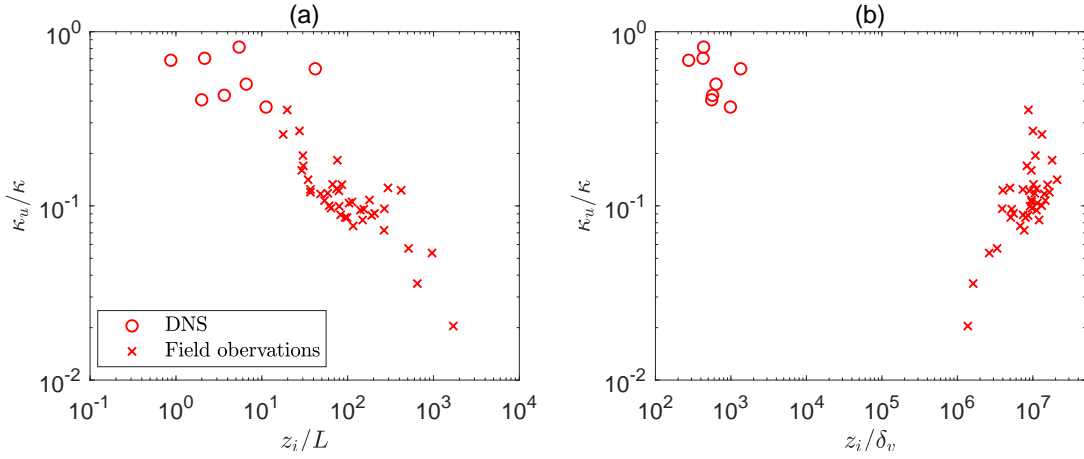


FIG. 4. The ratio $\frac{\kappa_u}{\kappa}$ plotted against (a) $\frac{z_i}{L}$, and (b) $\frac{z_i}{\delta_v}$ under various stably stratified conditions in DNS experiments and Cabauw observations.

$u_\tau \rightarrow 0$, the following asymptotic relation is required to cancel out u_τ :

$$\Phi\left(\frac{z_i}{\delta_v}, \frac{z_i}{L}\right) = \Phi\left(\frac{z_i}{L}\right) = \Phi\left(\frac{\kappa g z_i \theta_*}{\Theta_r u_\tau^2}\right) = c_1 \left(\frac{\kappa g z_i \theta_*}{\Theta_r u_\tau^2}\right)^{1/2}, \text{ for } \frac{z_i}{L} \rightarrow \infty, \quad (9)$$

where c_1 is a constant. Then the velocity gradient $\partial U/\partial z$ can then be rewritten as

$$\frac{\partial U}{\partial z} = c_1 \left(\frac{\kappa g z_i}{\Theta_r}\right)^{1/2} \frac{\theta_*^{1/2}}{z}, \text{ for } \frac{z_i}{L} \rightarrow \infty. \quad (10)$$

The above equation suggests that $\partial U/\partial z \rightarrow \infty$ as $z_i/L \rightarrow \infty$ and $\theta_* \rightarrow \infty$, corresponding to extreme stratified conditions. As $\kappa_u = 1/\Phi$, we can obtain

$$\kappa_u = \frac{1}{c_1} \left(\frac{z_i}{L}\right)^{-1/2}, \text{ for } \frac{z_i}{L} \rightarrow \infty. \quad (11)$$

The slope between κ_u and z_i/L obtained from Cabauw observations in the log-log plot is around -0.4 (Fig. 4a), which is not exactly the same as $-1/2$ based on the above equation. However, the asymptotic analysis still qualitatively captures the relation between κ_u and z_i/L in extreme stratified conditions at sufficiently high Reynolds number. It is worth noting that the extreme condition $z_i/L \rightarrow \infty$ is not observed in the Cabauw experiments, which might also be influenced by measurement uncertainties, thus leading to the difference between the observations and asymptotic analysis.

C. Discussion

The proposed velocity log law in the stably stratified boundary layers can be written as $\frac{\kappa_u z}{u_\tau} \frac{\partial U}{\partial z} = 1$, or equivalently,

$$\frac{\kappa z}{u_\tau} \frac{\partial U}{\partial z} = \kappa \Phi\left(\frac{z_i}{L}, \frac{z_i}{\delta_v}\right) = \frac{\kappa}{\kappa_u}, \quad (12)$$

where $\Phi\left(\frac{z_i}{L}, \frac{z_i}{\delta_v}\right)$ is independent of z and needs to be determined by numerical experiments or observations. According to MOST, the normalized velocity gradient was instead assumed to depend on z/L [9],

$$\frac{\kappa z}{u_\tau} \frac{\partial U}{\partial z} = \phi_m\left(\frac{z}{L}\right), \quad (13)$$

where ϕ_m is a stability correction function dependent on the distance to the wall z , thus leading to a non-logarithmic profile. The widely used Businger profile [77] for MOST is shown in Fig. 2, which is characterized by a slope rather than the observed plateau for $\frac{\kappa z}{u_\tau} \frac{\partial U}{\partial z}$. In numerical experiments, the function $\Phi\left(\frac{z_i}{L}, \frac{z_i}{\delta_v}\right)$ does not depend on z thus leading

to a log law. In our various stably stratified DNS datasets, $\frac{\kappa z}{u_\tau} \frac{\partial U}{\partial z}$ approaches a constant that is equal to $\frac{\kappa}{\kappa_u}$ (Fig. 2), thus supporting a log law rather than MOST. In addition, the slope of the proposed velocity log law depends on $\frac{z_i}{L}$ (buoyancy effects) and $\frac{z_i}{\delta_v}$ (Reynolds number effects). Such dependence of the slope on $\frac{z_i}{L}$ and $\frac{z_i}{\delta_v}$ has also been reported in temperature profiles in the convective boundary layers [38].

IV. CONCLUSION

We report new logarithmic velocity profiles in the near-wall region affected by buoyancy effects, through dimensional analysis, DNS experiments, and field observations of the stably stratified boundary layers. The new velocity log law can be described by $\frac{\kappa_u z}{u_\tau} \frac{\partial U}{\partial z} = 1$, where κ_u is a function of $\frac{z_i}{L}$ (buoyancy effects) and $\frac{z_i}{\delta_v}$ (Reynolds number effects) supported by both the DNS experiments and field observations. Asymptotic analysis for the slope κ_u has been conducted in the neutral limit and strongly stratified limit at sufficiently high Reynolds numbers. More accurate observations over a wider range of Reynolds numbers and stably stratified conditions may better constrain κ_u in the atmosphere. The proposed velocity log profile may replace Monin-Obukhov similarity function for velocity in global climate models and wall models for large eddy simulations, possibly leading to more realistic predictions of weather, climate, and hydrology, especially in polar regions.

ACKNOWLEDGMENTS

We would like to thank Dr. Kaighin McColl for helpful discussions. The computations in this paper were run on the FASRC Cannon cluster supported by the FAS Division of Science Research Computing Group at Harvard University. We would like to thank Dr. Fred C. Bosveld and Henk Klein Baltink for the help in obtaining the field data at the Cabauw Experimental Site for Atmospheric Research (<http://www.cesar-database.nl>).

[1] T. Kármán, von: Mechanische ähnlichkeit und turbulenz, nachr. ges. wiss. göttingen, math.-phys. kl.(1930) 58–76, Proc. 3. Int. Cong. Appl. Mech , 322 (1930).

- [2] C. B. Millikan, A critical discussion of turbulent flow in channels and circular tubes, in *Proc. 5th Int. Congress on Applied Mechanics (Cambridge, MA, 1938)* (Wiley, 1938) pp. 386–392.
- [3] B. J. McKeon, J.-d. Li, W. Jiang, J. F. Morrison, and A. J. Smits, Further observations on the mean velocity distribution in fully developed pipe flow, *J. Fluid Mech.* **501**, 135 (2004).
- [4] P. A. Monkewitz, K. A. Chauhan, and H. M. Nagib, Self-consistent high-reynolds-number asymptotics for zero-pressure-gradient turbulent boundary layers, *Phys. Fluids* **19**, 115101 (2007).
- [5] E. L. Andreas, K. J. Claffey, R. E. Jordan, C. W. Fairall, P. S. Guest, P. O. G. Persson, and A. A. Grachev, Evaluations of the von kármán constant in the atmospheric surface layer, *J. Fluid Mech.* **559**, 117 (2006).
- [6] M. Lee and R. D. Moser, Direct numerical simulation of turbulent channel flow up to $Re_\tau \approx 5200$, *J. Fluid Mech.* **774**, 395 (2015).
- [7] Y. Yamamoto and Y. Tsuji, Numerical evidence of logarithmic regions in channel flow at $Re_\tau = 8000$, *Phys. Rev. Fluids* **3**, 012602 (2018).
- [8] A. Obukhov, Turbulence in thermally inhomogeneous atmosphere, *Trudy Inst. Teor. Geofiz. Akad. Nauk SSSR* **1**, 95 (1946).
- [9] A. Monin and A. Obukhov, Basic laws of turbulent mixing in the surface layer of the atmosphere, *Contrib. Geophys. Inst. Acad. Sci. USSR* **151**, e187 (1954).
- [10] R. B. Stull, *An Introduction to Boundary Layer Meteorology*, Vol. 13 (Springer Science & Business Media, 1988).
- [11] J. W. Deardorff, Parameterization of the planetary boundary layer for use in general circulation models, *Mon. Weather Rev.* **100**, 93 (1972).
- [12] I. Troen and L. Mahrt, A simple model of the atmospheric boundary layer; sensitivity to surface evaporation, *Bound.-Layer Meteorol.* **37**, 129 (1986).
- [13] A. Holtslag and B. Boville, Local versus nonlocal boundary-layer diffusion in a global climate model, *J. Clim.* **6**, 1825 (1993).
- [14] J.-F. Louis, A parametric model of vertical eddy fluxes in the atmosphere, *Bound.-Layer Meteorol.* **17**, 187 (1979).
- [15] L. Mahrt, Stratified atmospheric boundary layers and breakdown of models, *Theor Comput Fluid Dyn* **11**, 263 (1998).

- [16] A. A. Grachev, E. L. Andreas, C. W. Fairall, P. S. Guest, and P. O. G. Persson, Similarity theory based on the doughterty–ozmidov length scale, *Q. J. R. Meteorol. Soc.* **141**, 1845 (2015).
- [17] P. Viterbo, A. Beljaars, J.-F. Mahfouf, and J. Teixeira, The representation of soil moisture freezing and its impact on the stable boundary layer, *Q. J. R. Meteorol. Soc.* **125**, 2401 (1999).
- [18] J. Cuxart, A. A. Holtslag, R. J. Beare, E. Bazile, A. Beljaars, A. Cheng, L. Conangla, M. Ek, F. Freedman, R. Hamdi, *et al.*, Single-column model intercomparison for a stably stratified atmospheric boundary layer, *Bound.-Layer Meteorol.* **118**, 273 (2006).
- [19] G. Svensson and A. A. Holtslag, Analysis of model results for the turning of the wind and related momentum fluxes in the stable boundary layer, *Bound.-Layer Meteorol.* **132**, 261 (2009).
- [20] A. Holtslag, G. Svensson, P. Baas, S. Basu, B. Beare, A. Beljaars, F. Bosveld, J. Cuxart, J. Lindvall, G. Steeneveld, *et al.*, Stable atmospheric boundary layers and diurnal cycles: challenges for weather and climate models, *Bull. Am. Meteorol. Soc.* **94**, 1691 (2013).
- [21] J. Teixeira, B. Stevens, C. Bretherton, R. Cederwall, J. D. Doyle, J.-C. Golaz, A. A. Holtslag, S. Klein, J. K. Lundquist, D. A. Randall, *et al.*, Parameterization of the atmospheric boundary layer: a view from just above the inversion, *Bull. Am. Meteorol. Soc.* **89**, 453 (2008).
- [22] G. Svensson, A. Holtslag, V. Kumar, T. Mauritsen, G. Steeneveld, W. Angevine, E. Bazile, A. Beljaars, E. De Bruijn, A. Cheng, *et al.*, Evaluation of the diurnal cycle in the atmospheric boundary layer over land as represented by a variety of single-column models: the second gabl experiment, *Bound.-Layer Meteorol.* **140**, 177 (2011).
- [23] M. M. Holland and C. M. Bitz, Polar amplification of climate change in coupled models, *Clim. Dyn.* **21**, 221 (2003).
- [24] L. Mahrt, Stably stratified atmospheric boundary layers, *Annu. Rev. Fluid Mech.* **46**, 23 (2014).
- [25] J. Forrer and M. Rotach, On the turbulence structure in the stable boundary layer over the greenland ice sheet, *Bound.-Layer Meteorol.* **85**, 111 (1997).
- [26] M. Pahlow, M. B. Parlange, and F. Porté-Agel, On monin–obukhov similarity in the stable atmospheric boundary layer, *Bound.-Layer Meteorol.* **99**, 225 (2001).
- [27] C. L. Klipp and L. Mahrt, Flux–gradient relationship, self-correlation and intermittency in the stable boundary layer, *Q.J.R. Meteorol. Soc.* **130**, 2087 (2004).

- [28] Y. Cheng, M. B. Parlange, and W. Brutsaert, Pathology of monin-obukhov similarity in the stable boundary layer, *J. Geophys. Res. Atmos.* **110** (2005).
- [29] A. A. Grachev, C. W. Fairall, P. O. G. Persson, E. L. Andreas, and P. S. Guest, Stable boundary-layer scaling regimes: the sheba data, *Bound.-Layer Meteorol.* **116**, 201 (2005).
- [30] C. Yagüe, S. Viana, G. Maqueda, and J. M. Redondo, Influence of stability on the flux-profile relationships for wind speed, ϕ_m , and temperature, ϕ_h , for the stable atmospheric boundary layer, *Nonlinear Process. Geophys.* **13**, 185 (2006).
- [31] J. Dougherty, The anisotropy of turbulence at the meteor level, *Journal of Atmospheric and Terrestrial Physics* **21**, 210 (1961).
- [32] R. Ozmidov, On the turbulent exchange in a stably stratified ocean. *izv. acad. sci. ussr, Atmos. Oceanic Phys.* **1**, 861 (1965).
- [33] A. Gargett, T. Osborn, and P. Nasmyth, Local isotropy and the decay of turbulence in a stratified fluid, *J. Fluid Mech.* **144**, 231 (1984).
- [34] M. L. Waite, Stratified turbulence at the buoyancy scale, *Phys. Fluids* **23**, 066602 (2011).
- [35] D. Li, S. T. Salesky, and T. Banerjee, Connections between the ozmidov scale and mean velocity profile in stably stratified atmospheric surface layers, *J. Fluid Mech.* **797** (2016).
- [36] Y. Cheng, Q. Li, S. Argentini, C. Sayde, and P. Gentine, A model for turbulence spectra in the equilibrium range of the stable atmospheric boundary layer, *J. Geophys. Res. Atmos.* **125**, e2019JD032191 (2020).
- [37] C. Tong and M. Ding, Multi-point monin-obukhov similarity in the convective atmospheric surface layer using matched asymptotic expansions, *J. Fluid Mech.* **864**, 640 (2019).
- [38] Y. Cheng, Q. Li, D. Li, and P. Gentine, Logarithmic profile of temperature in sheared and unstably stratified atmospheric boundary layers, *Phys. Rev. Fluids* **6**, 034606 (2021).
- [39] O. Flores and J. Riley, Analysis of turbulence collapse in the stably stratified surface layer using direct numerical simulation, *Bound.-Layer Meteorol.* **139**, 241 (2011).
- [40] C. Ansorge and J. P. Mellado, Global intermittency and collapsing turbulence in the stratified planetary boundary layer, *Bound.-Layer Meteorol.* **153**, 89 (2014).
- [41] G. Ahlers, E. Bodenschatz, D. Funfschilling, S. Grossmann, X. He, D. Lohse, R. J. Stevens, and R. Verzicco, Logarithmic temperature profiles in turbulent rayleigh-bénard convection, *Phys. Rev. Lett.* **109**, 114501 (2012).

- [42] S. Grossmann and D. Lohse, Logarithmic temperature profiles in the ultimate regime of thermal convection, *Phys. Fluids* **24**, 125103 (2012).
- [43] G. Ahlers, E. Bodenschatz, and X. He, Logarithmic temperature profiles of turbulent rayleigh–bénard convection in the classical and ultimate state for a prandtl number of 0.8, *J. Fluid Mech.* **758**, 436 (2014).
- [44] M. Hölling and H. Herwig, Asymptotic analysis of the near-wall region of turbulent natural convection flows, *J. Fluid Mech.* **541**, 383 (2005).
- [45] C.-H. Moeng, A large-eddy-simulation model for the study of planetary boundary-layer turbulence, *J. Atmos. Sci.* **41**, 2052 (1984).
- [46] J. W. Deardorff, Numerical investigation of neutral and unstable planetary boundary layers, *J. Atmos. Sci.* **29**, 91 (1972).
- [47] F. T. Nieuwstadt, P. J. Mason, C.-H. Moeng, and U. Schumann, Large-eddy simulation of the convective boundary layer: A comparison of four computer codes, in *Turbulent shear flows 8* (Springer, 1993) pp. 343–367.
- [48] Q. Li, P. Gentine, J. P. Mellado, and K. A. McColl, Implications of nonlocal transport and conditionally averaged statistics on monin–obukhov similarity theory and townsend’s attached eddy hypothesis, *J. Atmos. Sci.* **75**, 3403 (2018).
- [49] J.-P. Mellado, C. Bretherton, B. Stevens, and M. Wyant, Dns and les for simulating stratocumulus: better together, *J. Adv. Model. Earth Syst.* **10**, 1421 (2018).
- [50] M. Jiménez and J. Cuxart, Large-eddy simulations of the stable boundary layer using the standard kolmogorov theory: Range of applicability, *Bound.-Layer Meteorol.* **115**, 241 (2005).
- [51] H. Schmidt and U. Schumann, Coherent structure of the convective boundary layer derived from large-eddy simulations, *J. Fluid Mech.* **200**, 511 (1989).
- [52] S. Khanna and J. G. Brasseur, Analysis of monin–obukhov similarity from large-eddy simulation, *J. Fluid Mech.* **345**, 251 (1997).
- [53] E. Bou-Zeid, C. Meneveau, and M. Parlange, A scale-dependent lagrangian dynamic model for large eddy simulation of complex turbulent flows, *Phys. Fluids* **17**, 025105 (2005).
- [54] Y. Cheng, C. Sayde, Q. Li, J. Basara, J. Selker, E. Tanner, and P. Gentine, Failure of taylor’s hypothesis in the atmospheric surface layer and its correction for eddy-covariance measurements, *Geophys. Res. Lett.* **44**, 4287 (2017).

- [55] R. J. Beare, M. K. Macvean, A. A. Holtslag, J. Cuxart, I. Esau, J.-C. Golaz, M. A. Jimenez, M. Khairoutdinov, B. Kosovic, D. Lewellen, *et al.*, An intercomparison of large-eddy simulations of the stable boundary layer, *Bound.-Layer Meteorol.* **118**, 247 (2006).
- [56] S. Khani and M. L. Waite, Buoyancy scale effects in large-eddy simulations of stratified turbulence, *J. Fluid Mech.* **754**, 75 (2014).
- [57] P. P. Sullivan, J. C. Weil, E. G. Patton, H. J. Jonker, and D. V. Mironov, Turbulent winds and temperature fronts in large-eddy simulations of the stable atmospheric boundary layer, *J. Atmos. Sci.* **73**, 1815 (2016).
- [58] S. K. Shah and E. Bou-Zeid, Direct numerical simulations of turbulent ekman layers with increasing static stability: modifications to the bulk structure and second-order statistics, *J. Fluid Mech.* **760**, 494 (2014).
- [59] S. I. Gohari and S. Sarkar, Direct numerical simulation of turbulence collapse and rebirth in stably stratified ekman flow, *Bound.-Layer Meteorol.* **162**, 401 (2017).
- [60] C. C. v. Heerwaarden, B. J. Van Stratum, T. Heus, J. A. Gibbs, E. Fedorovich, and J. P. Mellado, Microhh 1.0: a computational fluid dynamics code for direct numerical simulation and large-eddy simulation of atmospheric boundary layer flows, *Geosci. Model Dev.* **10**, 3145 (2017).
- [61] G. Coleman, J. Ferziger, and P. Spalart, Direct simulation of the stably stratified turbulent ekman layer, *J. Fluid Mech.* **244**, 677 (1992).
- [62] A. N. Kolmogorov, The local structure of turbulence in incompressible viscous fluid for very large reynolds numbers, *Dokl. Akad. Nauk SSSR* **30**, 299 (1941).
- [63] A. Apituley, H. Russchenberg, H. van der Marel, F. Bosveld, R. Boers, H. ten Brink, G. de Leeuw, R. Uijlenhoet, B. Arbresser-Rastburg, and T. Rockmann, Overview of research and networking with ground based remote sensing for atmospheric profiling at the cabauw experimental site for atmospheric research (cesar)-the netherlands, in *IGARSS 2008-2008 IEEE International Geoscience and Remote Sensing Symposium*, Vol. 3 (IEEE, 2008) pp. III–903.
- [64] F. C. Bosveld, P. Baas, A. C. Beljaars, A. A. Holtslag, J. V.-G. de Arellano, and B. J. Van De Wiel, Fifty years of atmospheric boundary-layer research at cabauw serving weather, air quality and climate, *Bound.-Layer Meteorol.* **177**, 583 (2020).
- [65] L. Choma, T. Musil, H. Némethová, J. Jevčák, P. Petříček, S. Makó, M. Pilát, and F. Balla, Comparative analysis of selected ceilometers for practice and academic purposes, in *2019*

- Modern Safety Technologies in Transportation (MOSATT)* (IEEE, 2019) pp. 35–38.
- [66] J. C. Wyngaard, *Turbulence in the Atmosphere* (Cambridge University Press, 2010).
- [67] W. K. George, Is there a universal log law for turbulent wall-bounded flows?, *Philos. Trans. R. Soc. A* **365**, 789 (2007).
- [68] I. Marusic, J. P. Monty, M. Hultmark, and A. J. Smits, On the logarithmic region in wall turbulence, *J. Fluid Mech.* **716** (2013).
- [69] T. Foken, 50 years of the monin–obukhov similarity theory, *Bound.-Layer Meteorol.* **119**, 431 (2006).
- [70] H. A. Panofsky, Determination of stress from wind and temperature measurements, *Q. J. R. Meteorol. Soc.* **89**, 85 (1963).
- [71] G. Kramm, D. J. Amaya, T. Foken, *et al.*, Hans a. panofsky’s integral similarity function—at fifty, *Atmospheric and Climate Sciences* **2013** (2013).
- [72] F. T. Nieuwstadt, The turbulent structure of the stable, nocturnal boundary layer, *J. Atmos. Sci.* **41**, 2202 (1984).
- [73] L. Mahrt, Vertical structure and turbulence in the very stable boundary layer, *J. Atmos. Sci.* **42**, 2333 (1985).
- [74] L. Mahrt and D. Vickers, Extremely weak mixing in stable conditions, *Bound.-Layer Meteorol.* **119**, 19 (2006).
- [75] L. Mahrt, The near-calm stable boundary layer, *Bound.-Layer Meteorol.* **140**, 343 (2011).
- [76] S. Pope, *Turbulent Flows* (Cambridge University Press, 2000).
- [77] J. A. Businger, J. C. Wyngaard, Y. Izumi, and E. F. Bradley, Flux-profile relationships in the atmospheric surface layer, *J. Atmos. Sci.* **28**, 181 (1971).
- [78] O. Williams, T. Hohman, T. Van Buren, E. Bou-Zeid, and A. J. Smits, The effect of stable thermal stratification on turbulent boundary layer statistics, *J. Fluid Mech.* **812**, 1039 (2017).